

A Physical Basis of Predicting the Magnitude and Failure Time of a Forthcoming Earthquake

Jeen-Hwa Wang^{1,2}

⁽¹⁾ Institute of Earth Sciences, Academia Sinica, Taipei, Taiwan

⁽²⁾ Department of Earth Sciences, National Central University, Jhongli, Taiwan

Article history: received November 4, 2022; accepted March 27, 2023

Abstract

Let T and M be, respectively, the precursor time of a certain precursor and the magnitude of a forthcoming earthquake. Observations may lead to a relationship of T versus M in a form of $\log(T) = a + bM$. Based on the $\log(T)$ - M relationships of two different precursors inferred from observed data, we propose a new method of predicting the magnitude and failure time of a forthcoming earthquake. In the study, we will explore the intrinsic physics of a $\log(T)$ - M relationship and explain the constraints and requirements on the two $\log(T)$ - M relationships for prediction. In addition, we will give a testing example based on the $\log(T)$ - M relationships inferred from the data of presismic radon concentration anomalies and gamma-ray emission changes observed at respective monitoring stations in Taiwan. Results confirm a high possibility of predicting the magnitude and failure time of a forthcoming earthquake just from the observed occurrence times of two different precursors based on their $\log(T)$ - M relationships.

Keywords: Earthquake precursor; Precursor time; Earthquake magnitude; Failure time; Relationship of precursor time versus magnitude

1. Introduction

One of the significant ways to reduce seismic hazards is the successful prediction or forecasting of forthcoming earthquakes from observations of reliable precursors. Of course, this is a challenging problem [e.g., Knopoff, 1996]. Aki [1989, 2009] assumed that earthquakes are predictable and also suggested that earthquake scientists would inform the probability of the occurrence of an earthquake with a specified magnitude, place, and time window to the government and the public. An earthquake, especially for the large one, is usually preceded by complex physical and chemical processes which may behavior as the precursors [e.g., Atkinson, 1984; Main and Meredith, 1989]. Hence, earthquake prediction or forecasting should be based on physics [e.g., Field, 2019; Segou, 2020; and cited references therein]. When a certain precursor appears, the time window is merely the precursor time, T , of this precursor [e.g., Wang et al., 2016; Wang, 2021a, 2021b]. The precursor time is measured from the occurrence time of a precursor to the failure time of the forthcoming earthquake. Of course, the precursor times may be different for distinct precursors.

A significant physical characteristic of observed precursors is the presence of a linear relationship between $\log(T)$ for a precursor or several precursors and the magnitude, M , of a forthcoming earthquake in the form: $\log(T) = a + bM$ where a and b are two coefficients. Note that in order to avoid the possible confusion with the coefficient b of the $\log(T)$ – M relationship, the coefficient of the Gutenberg-Richter's frequency-magnitude law [Gutenberg and Richter, 1944] is denoted as ' B ' in the followings. The $\log(T)$ – M relationship has been recognized from the observations for a long time by numerous authors [e.g., Scholz et al., 1973; Whitcomb et al., 1973; Rikitake, 1975a]. From the plot of T (in days) versus M for five precursors (crustal movements, electric resistivity, radon (denoted as Rn hereafter) emission, v_p/v_s anomaly, and B -value) from 30 world-wide earthquakes, Scholz et al. [1973] inferred a relationship: $M = -5.81 + 1.55\log(T)$ (T in days) which gives $\log(T) = 3.75 + 0.65M$. For the precursors of crustal deformations and seismic-wave velocities, Whitcomb et al. [1973] obtained $\log(T) = -1.92 + 0.80M$ (T in days).

Although earthquake prediction seems successful for few large events, including the 1975 Haicheng, China, earthquake [e.g., Wang et al., 2006], earthquake prediction is still debatable. Numerous scientists do not believe that earthquakes can be predicted [e.g., Geller, 1996, 1997; Geller et al., 1997]. This problem might be caused by several reasons. That the relationships of $\log(T)$ versus M as reported by Scholz et al. [1973] and Whitcomb et al. [1973] are not universal might be one of the possible reasons. From a plot of $\log(T)$ versus M for Rn concentration anomalies observed in different tectonic provinces, Hauksson [1981] could not infer a linear $\log(T)$ – M relationship like those reported by Scholz et al. [1973] and Whitcomb et al. [1973] due to large dispersion of data points even though $\log(T)$ increases with M .

In Japan, Tsubokawa [1969, 1973] first obtained a linear relation between the precursor time of crustal movement and magnitude of mainshock in the form: $\log(T) = -1.88 + 0.79M$. After analyzed the data of various earthquake precursors, including land deformation, tilt and strain, foreshocks, B -value of the frequency-magnitude relationship, micro-seismicity, source mechanism, fault creep anomaly, v_p and v_s (v_p = the P-wave velocity and v_s = the S-wave velocity), v_p/v_s , geomagnetism, earth current, resistivity, radon, underground water, and oil flow) amounting to 418 in number, Rikitake [1975b, 1976] related the precursor time of a precursor to the magnitude, M , of the forthcoming mainshock in the following equation: $\log(T) = -1.83 + 0.76M$. He stressed that the $\log(T)$ – M relationships are different for different groups of precursors. From a data set of 391 cases of precursors, Rikitake [1979, 1984] divided the data into three classes. Excluding the third class for foreshocks, tilt and strain, and earth's currents, he obtained $\log(T) = -1.01 + 0.60M$ (T in days) for the first class including 192 cases and $\log(T) = -1.0$ for the second class. Clearly the second class of precursors includes almost the imminent precursors that appeared about one day immediately before the forthcoming earthquakes. For the third class, the frequencies of $\log(T)$ are distributed in a very wide range with two peaks: one at $\log(T) = 1.0$ and the other at $\log(T) = -1.0$. From the preseismic earth resistivity changes before 30 large Japanese earthquakes with $4.7 \leq M \leq 7.9$, Rikitake and Yamazaki [1985] inferred the following equation: $\log(T) = 0.41M - 1.6\log(R)$ (T in days) where R (in km) is the hypocentral distance. In New Zealand, Smith [1981, 1986] obtained the following relationship: $\log(T) = 1.42 + 0.30M$ from the data of abnormal B -values. In China, Ding et al. [1985] inferred the following relationship: $\log(T) = -0.34 + 0.38M$ for various precursors proceeding large Chinese earthquakes. From the data of Rn concentration anomalies for six earthquakes with $M_w = 5.0$ – 6.8 and $d = 7.0$ – 35.6 km (d = the focal depth, in km) occurred in southeastern Taiwan, Kuo et al. [2020] obtained $\log(T) = 1.456 + 0.053M_w$. From the data of Rn concentration anomalies for more than one hundred earthquakes with $4 \leq M_L < 8$ (M_L = the local magnitude) in Taiwan, Wang [2021b] inferred the relationships (T in days): $\log(T) = (-2.05 \pm 0.40) + (0.58 \pm 0.01)M_L$ for the events with $d \leq 40$ km and $\log(T) = (-0.40 \pm 0.42) + (0.26 \pm 0.01)M_L$ for the events with $d > 40$ km. From the data of b -value anomalies for 45 world-wide earthquakes with $3 \leq M_s \leq 9$ (M_s = the surface-wave magnitude), Wang et al. [2016] inferred the relationship (T in years): $\log(T) = (2.02 \pm 0.49) + (0.15 \pm 0.07)M_s$.

Clearly the $\log(T)$ – M relationships inferred by Rikitake [1979, 1984], Smith [1981, 1986], Wang et al. [2016], Kuo et al. [2020], and Wang [2021b] are remarkably different from one another and also different from those obtained by Scholz et al. [1973] and Whitcomb et al. [1973]. This indicates that the $\log(T)$ – M relationships reported by Scholz et al. [1973] and Whitcomb et al. [1973] are not universal. In addition, the $\log(T)$ – M relationship for the B -value anomalies inferred by Smith [1981, 1986] for New-Zealand earthquakes is different from that done by Wang et al. [2016] for world-wide events. Wang [2021b] also addressed the difference between the world-wide earthquakes and Taiwan events. Of course, the large variance of the inferred relations for different precursors that were obtained from different areas may be due to absence of robustness, biased identification of a statistically weak relation, poor data quality and manipulation, and numerous other reasons, including regional-dependence. Hence, the $\log(T)$ – M relationships may vary for different types of precursors and also for distinct tectonic regions.

In other word, the time window of earthquake prediction should depend on the observed precursor and may change from one precursor to the other. However, up to date the $\log(T)$ - M relationships have been inferred only for some precursors in few seismically active regions.

The existence of distinct $\log(T)$ - M relationships for different types of precursors are significant for practical earthquake prediction. In this study, we will first discuss the intrinsic physics of the $\log(T)$ - M relationships and then explore the physical basis of predicting the magnitude and failure time, t_r , of a forthcoming earthquake based on the $\log(T)$ - M relationships of two different precursors. In addition, the $\log(T)$ - M relationships of presismic radon (denoted by R_n hereafter) concentration anomalies and gamma-ray (written as γ -ray hereafter) emission changes observed in Taiwan will be taken as a testing example.

2. Intrinsic Physics of the Relationship of T versus M

2.1 The Correlation of Precursor Time to Fault Length

Numerous authors [e.g., Nur, 1972; Aggarwal et al., 1973; Scholz et al., 1973; Whitcomb et al., 1973; Anderson and Whitcomb, 1975; Rikitake, 1975a; Enomoto, 2012; Wang, 2016] considered a mechanism involving the diffusion of fluids and gas flows in the cracks along the fault's zones in and near the source area, thus yielding anomalies of seismic-wave velocities, B -values, electromagnetic radiation, etc. Aggarwal et al. [1973] Scholz et al. [1973], and Whitcomb et al. [1973] assumed that T correlates to L where L is either the characteristic length of the aftershock area or the linear dimension of the fault area of the forthcoming earthquake in the following form: $T \sim L^\kappa$ where κ is the scaling exponent.

Aki [1966] defined the seismic moment as $M_o = \mu \bar{u} A$ where μ , \bar{u} , and A are the rigidity of fault rocks, the average displacement on the source area, and the source area, respectively. Purcaru and Berckhemer [1978] obtained a relationship between M_o and M as described below:

$$\log(M_o) = 16.1 + 1.5M. \quad (1)$$

The scaling law of M_o versus L that is the fault length is [e.g., Kanamori and Anderson, 1975; Scholz, 1990; Wang, 2018]: $M_o \sim L^n$ where n is 2 for small and medium-sized events that rupture in the 2-D domain and 1 for larger-sized events that rupture mainly in the 1-D domain usually along the horizontal direction. Inserting this scaling law into Equation (1) leads to $M \sim (2n/3)\log(L)$ and thus $\log(T) \sim (2nb/3)\log(L)$. Letting κ to be $2nb/3$, we have

$$T \sim L^\kappa. \quad (2)$$

Equation (2) indicates that the precursor time is dependent on the fault length of the forthcoming earthquake. Clearly different precursors with distinct values of b may have different precursor times from Equation (2). The scaling exponent n between M_o and L is also a factor in influencing T . Although n is 2 times smaller for a larger-sized earthquake than for a small or medium-sized event as mentioned above, the value of T for a certain precursor may still be longer for the former than for the latter because L is commonly longer (even much longer) for the former than for the latter.

The value of κ is 1.6 inferred by Aggarwal et al. [1973] and ~ 2.0 by both Scholz et al. [1973] (based on the linear dimension of the aftershock area of the mainshock) and Whitcomb et al. [1973] (based on the linear dimension of the source area of the mainshock). Considering $\kappa = 1.6$, the value of $b = 3\kappa/2n$ are 2.4 for $n = 1$ and 1.2 for $n = 2$. Clearly b is larger than 1 and should be bigger as $\kappa = 2$. However, the results observed by numerous authors, even including Scholz et al. [1973] and Whitcomb et al. [1973], as mentioned above, show $b < 1.0$. This seems to suggest that the values of κ inferred by both Scholz et al. [1973] and Whitcomb et al. [1973] for several precursors from some earthquakes cannot be universal. Dieterich [1978] stated that $\kappa = 2$ inferred by Whitcomb et al. [1973] was due to the use of estimated values of L based on the M - L relationship given by Wyss and Brune [1968] who only

took small and medium-sized earthquakes. Dieterich [1978] used the M - L relationship inferred by Press [1967] to evaluate L , and thus he obtained $\kappa = 1$. This suggests that large κ might be due to either over-estimates of fault lengths of large earthquakes or under-estimates of those of small and medium-sized events. The value of $\kappa = 1$ leads to $b = 0.75$ for $n = 2$. This b value is comparable with $b = 0.65$ inferred by Scholz et al. [1973] and $b = 0.80$ done by Whitcomb et al. [1973]. As considering the characteristic length of aftershock area, A , [e.g., Scholz et al., 1973], we must concern the selection of the optimum time to evaluate the value of A for evaluation L ($\sim A^{1/2}$). This is due to three reasons [see Tajima and Kanamori, 1985]: (1) the aftershocks expand outwards with time from the source area of the mainshock; (2) the expanding rate may vary with time; and (3) the expanding rates are different for distinct earthquakes. These reasons would affect the estimates of the characteristic lengths, L , for different mainshocks. The $\log(L)$ - M relationships that are usually in the form of $\log(L) = a' + b'M$ may be different for the earthquakes occurring in distinct tectonic regions [e.g., Utsu and Seki, 1955; Hsu, 1971; Kagan, 2002; Konstantinos et al., 2005]. Hsu [1971] addressed that the $\log(L)$ - M relationship for the earthquakes in Taiwan cannot be described by the above-mentioned linear form. These reasons would influence the estimate of κ . Since b is commonly smaller than 1 from numerous observations as mentioned above, κ could not be higher than 1. In addition, Dieterich [1978] applied the stress, σ , and slip, u in the preseismic processes to interpret the $\log(T)$ - M relationship. Consequently, the inference of the L - M relationship is important for the evaluation of κ . Of course, the reliable inference is more important for the T - M relationship than for the L - M one for the following study.

2.2 The Correlation of Precursor Time to Strain Energy

The Gutenberg-Richter's energy-magnitude law of earthquakes [Gutenberg and Richter, 1942, 1956] is:

$$\log(E_s) = 11.8 + 1.5M \quad (3)$$

which E_s is the seismic-wave energy and M is commonly the surface-wave magnitude, M_s . Equation (3) gives $M \sim (2/3) \log(E_s)$. From $\log(T) = a + bM$, we have

$$\log(T) \sim bM \sim (2b/3) \log(E_s). \quad (4)$$

Since $E_s = \eta \Delta E$ where ΔE is the strain energy of an earthquake and η (< 1) is the seismic efficiency [cf. Wang, 2004], we have

$$T \sim \Delta E^{2b\eta/3}. \quad (5)$$

Equation (5) indicates that the precursor time is dependent on the strain energy of the forthcoming earthquake. Obviously different precursors with distinct values of b may have different precursor times from Equation (5) for a forthcoming earthquake. The seismic efficiency that depends on the physical and chemical properties of the fault-zone rocks [cf. Knopoff, 1958; Kanamori and Heaton, 2000; Wang, 2009] may also influence T .

The Benioff strain is defined to be $S = (E_s)^{1/2}$ for a single event [cf. Bufe and Varnes, 1993]. The Benioff strain release diagram has been used to represent accelerated fracture release before earthquakes [e.g., Wyss, 2001; Papazachos and Papazachos, 2001; Papazachos et al., 2002; Scordilis et al., 2004; Sarkar, 2010; Frid et al., 2011]. Jaume and Sykes [1999] addressed that preseismic changes in the Benioff strain release were equivalent to those observed in experimental rock fracture. Bufe and Varnes [1993] claimed that we could accurately predict the failure time of a forthcoming earthquake from the cumulative Benioff strain release diagram. Of course, the diagram cannot lead to the size of the event. Numerous authors also related it to preseismic precursors, for example, the electromagnetic radiations [e.g., Frid and Vozoff, 2005; Frid et al., 2011]. Hence, the precursors appear during the

Benioff strain release processes. The time period of the processes should be longer for larger forthcoming earthquake with Benioff strain of S . Here we may consider the correlation between T and S for a forthcoming earthquake. From Equation (4), we have

$$T \sim S^{4b/3}. \quad (6)$$

Equation (6) indicates that the precursor time is dependent on the Benioff strain of the forthcoming earthquake. Obviously different precursors with distinct values of b may have different precursor times from Equation (6) for a forthcoming earthquake.

Equations (2), (5), and (6) exhibit the power-law relationship between the precursor time, T , and the characteristic length of a fault area, L , that between T and the strain energy, ΔE , and that between T and the Benioff strain, S , respectively. Numerous time-dependent earthquake phenomena exhibit the power-law behavior [e.g., Omori, 1894; Aki, 1967; Wang and Lee, 1997; Wang, 2013, 2014]. This might indicate the existence of memory effect in time-dependent earthquake phenomena [cf. Wang, 2017; Meng et al., 2019]. That the precursors randomly occur and are not related to the forthcoming earthquake means a lack of memory effect. This would yield high difficulty or low possibility of predicting forthcoming earthquakes. Hence, we assume that the memory effect must be one of the fundamental requests of successful earthquake prediction. Therefore, the presence of positive linear correlation between $\log(T)$ (for the precursors) and M (for the forthcoming earthquake) directly shows the memory effect, thus leading to high reliability of earthquake prediction.

3. Physical Basis of a Method of Earthquake Prediction

3.1 Theoretical Basis

Considering two different precursors, the $\log(T)$ - M relationship for the i -th precursor ($i = 1$ and 2) is represented as the following form:

$$\log(T_i) = a_i + b_i M \quad (7)$$

or

$$T_i = 10^{(a_i + b_i M)} \quad (8)$$

where $T_i = t_r - t_i$, t_r = the failure time of a forthcoming earthquake, and t_i = the occurrence time of the i -th precursor. As mentioned previously, the coefficients a_i and b_i are dependent on the type of precursors and also of regional-dependence.

We here propose a method to evaluate the two unknowns t_r and M from Equation (7) or Equation (8). For this method, we need two $\log(T)$ - M relationships of different precursors. Considering two different precursors whose occurrence times are t_1 and t_2 , respectively, Equation (7) gives

$$\log(t_r - t_1) = a_1 + b_1 M \quad (9)$$

for the first precursor and

$$\log(t_r - t_2) = a_2 + b_2 M \quad (10)$$

for the second one. Equation (9) and Equation (10), respectively, lead to

$$t_r = t_1 + 10^{(a_1 + b_1 M)}; \quad (11)$$

and

$$t_r = t_2 + 10^{(a_2 + b_2 M)}. \quad (12)$$

Equality of the two equations yields

$$t_1 + 10^{(a_1 + b_1 M)} = t_2 + 10^{(a_2 + b_2 M)}. \quad (13)$$

Defining $F_1(M) = t_1 + 10^{(a_1 + b_1 M)}$ and $F_2(M) = t_2 + 10^{(a_2 + b_2 M)}$, Equation (13) gives $F_1(M) = F_2(M)$. We may solve the value of M from this equality through the following technique because t_1, a_1, b_1, t_2, a_2 and b_2 are known.

Considering that the second precursor occurred almost simultaneously with or later than the first one, we have $t_2 \geq t_1$. This makes Equation (13) becomes

$$10^{(a_1 + b_1 M)} - 10^{(a_2 + b_2 M)} = t_2 - t_1 \geq 0. \quad (14)$$

Equation (14) leads to $10^{(a_1 + b_1 M)} > 10^{(a_2 + b_2 M)}$ or $a_1 + b_1 M > a_2 + b_2 M$. This yields

$$(b_1 - b_2)M \geq a_2 - a_1. \quad (15)$$

Although the value of M may be negative for very small natural events, only large, positive M is considered here because we are only interested in the prediction of medium-sized and large earthquakes.

Examples of the two curves associated with the two functions that are normalized by the maximum value of either $F_1(M)$ or $F_2(M)$ are schematically plotted in Figure 1 with $t_1 = 10$ days and $t_2 = 15$ days for $M = 1-9$. In the figure, $F_1(M)$ and $F_2(M)$ are displayed by a solid line and a dashed line, respectively. Note that in the four panels, the difference between $F_1(M=1)$ and $F_2(M=1)$ is very small because the maximum value of either $F_1(M=9)$ or $F_2(M=9)$ is relatively very large. We may numerically evaluate the value of M from the intersection point between the two curves. When M has been estimated, the value of t_r is either $t_1 + 10^{(a_1 + b_1 M)}$ or $t_2 + 10^{(a_2 + b_2 M)}$. Hence, we may predict M and t_r of the forthcoming earthquake.

From Equation (15), if $a_2 - a_1 > 0$ or $a_1 < a_2$, $b_1 - b_2$ must be positive and thus $b_1 > b_2$. Hence, the two inequalities, i.e., $a_2 < a_1$ and $b_1 > b_2$, form the first condition such that M can be solved from Equation (13). An example is displayed in Figure 1a where the two curves intersect at a certain M , thus leading to the solution. If $a_2 - a_1 = 0$ or $a_1 = a_2$, $b_1 - b_2$ must be positive and thus $b_1 > b_2$. An example is displayed in Figure 1b. The two curves cannot intersect each other when $M > 1$ because the increasing rate is higher for $F_1(M)$ than for $F_2(M)$ due to $b_1 > b_2$. If $a_2 - a_1 < 0$ or $a_1 > a_2$, $b_1 - b_2$ may be positive, i.e., $b_1 > b_2$, or zero, i.e., $b_1 = b_2$, or negative, i.e., $b_1 < b_2$. For $b_1 > b_2$, an example is displayed in Figure 1c. The two curves cannot intersect each other at a certain M when $M > 1$ because the increasing rate is higher for $F_1(M)$ than for $F_2(M)$ due to $b_1 > b_2$. Like $b_1 > b_2$, the two curves may intersect each other at a certain M when $b_1 = b_2$. For $b_1 < b_2$, there are two possibilities. The first possibility is that the value of M may be solved from Equation (13) for $M < (a_1 - a_2)/(b_2 - b_1)$. An example for this condition is displayed in Figure 1d. Clearly, the two curves may intersect each other at a large value of M , thus leading to the solution. The second possibility is that the inequality $M < (a_1 - a_2)/(b_2 - b_1)$ does not hold or holds only for either negative M or small M . This does not make M be solved from Equation (13). Consequently, the value of M of a forthcoming mainshock may be solved from Equation (13) under either the first condition of $a_1 < a_2$ and $b_1 > b_2$ or the second one of $a_1 > a_2$ and $b_1 \leq b_2$. Then, the failure time, i.e., t_r , of the forthcoming mainshock may be evaluated from either Equation (11) or Equation (12).

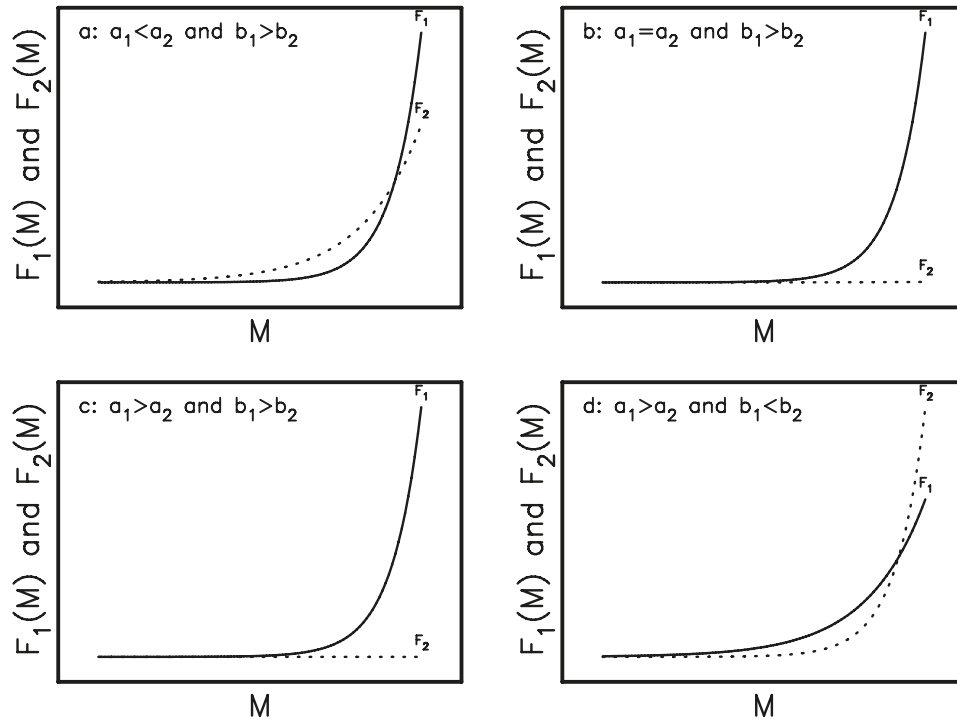


Figure 1. The non-scaled curves of for $F_1(M)$ and $F_2(M)$ with $t_2 > t_1$: (a) for $a_1 < a_2$ and $b_1 > b_2$; (b) for $a_1 = a_2$ and $b_1 > b_2$; (c) for $a_1 > a_2$ and $b_1 > b_2$; and (d) for $a_1 > a_2$ and $b_1 < b_2$ under the constrain: $M < (a_1 - a_2)/(b_2 - b_1)$.

3.2 Three Requirements

Based on the above-mentioned theory, we may predict the magnitude and failure time of a forthcoming earthquake when the relationships of $\log(T)$ versus M of two different precursors are reliable. Nevertheless, we should still pay attention to the following three important requirements that will influence the feasibility and reliability of the present theory for predicting earthquakes.

The first requirement is that we must collect related data and construct, at least, two different $\log(T)$ – M relationships for a certain study region. As mentioned above, the $\log(T)$ – M relationships for a certain precursor could be regional-dependent. According to the differences in tectonic and geological conditions, it might be not appropriate to apply the relationships obtained from other regions or to use the average relationships inferred from world-wide earthquakes to a certain study region.

The second requirement is that the precursor times of the two precursors in use must be in the same order of magnitude. It is inappropriate to compare the power-law function of $\log(T)$ versus M of a precursor whose value of T is in the unit of days with that of a precursor whose value of T is in the unit of years. Otherwise, this will yield a large value of $t_2 - t_1$, thus being unable to make the two curves intersect each other at a point as shown in Fig. 1 because of remarkable separation between them. In other word, the values of t_1 and t_2 should be reliable and $t_2 - t_1$ cannot be too big.

The third requirement is that it is necessary to consider the standard deviations δa_i and δb_i , respectively, for a_i and b_i which commonly exist because the $\log(T)$ – M relationship is inferred from the observations with errors as shown in the previous examples. If the values of δa_i and δb_i are larger due to insufficient or lowly reliable data, the errors of evaluated values of M and t_r , especially for the latter, should be bigger, thus leading to higher uncertainty of prediction.

4. A Testing Example and Discussion

4.1 Evaluation of the Magnitude of a Forthcoming Earthquake

Numerous earthquake precursors have been long observed and studied in Taiwan [e.g., Tsai et al., 1983, 2004, 2018; Wang, 2021b]. Rn concentration anomalies are usually taken as a significant precursor of earthquakes [e.g., Teng, 1980; Wakita et al., 1985; King, 1986; Wakita, 1996; King et al., 2006; Woith, 2015; Paudel et al., 2018]. Taiwan's geochemists installed numerous automatically monitoring stations for measuring Rn concentrations in the field. One of the stations is the TPT station as illustrated by with an open triangle in Figure 2. The gamma-ray (denoted as γ -ray hereafter) emission is mainly produced from the radioactive decay of Rn or from thunderstorms [e.g., Tsukuda, 2008; Minnehan, 2015]. Four stations for automatically monitoring γ -ray emissions have been installed in Taiwan [Fu et al., 2015]. One station is the YMSG station that is installed at the Taiwan Volcano Observatory (TVO) in Mt. Yangming, Northern Taiwan and illustrated by an open diamond symbol in Fig. 2. For numerous earthquakes, Rn concentration anomalies and γ -ray emission changes have been measured on the respective stations by local geochemists. The authors, who made the measures of anomalies, addressed that the two kinds of precursors are physically, chemically, and geologically related to earthquakes. Hence, the $\log(T)$ - M relationships for the two precursors may be established.

In the followings, the source parameters of earthquakes in use are taken from the data base provided by the Central Weather Bureau (CWB), Taiwan. The earthquake magnitude is the local magnitude, M_L [Shin, 1992]. The focal depth of an earthquake is denoted by d (in km) and the epicentral distance from an event to an observation station is represented by Δ (in km).

At the YMSG station, Fu et al. [2019] observed γ -ray emission changes before 20 events with $M_L = 2.8$ – 6.7 happened during July 1, 2014 to June 1, 2015. The precursor times are 2–20 days. Meanwhile, they also observed Rn concentration anomalies before 15 events with $M_L = 2.3$ – 6.7 at the station TPT. The precursor times are 1–23 days. Totally, there are 25 events having either Rn concentration anomalies or γ -ray emission changes. Ten of the 25 events have the two precursors simultaneously. The related data of the 25 events are listed in Table 1 and their epicenters are plotted in

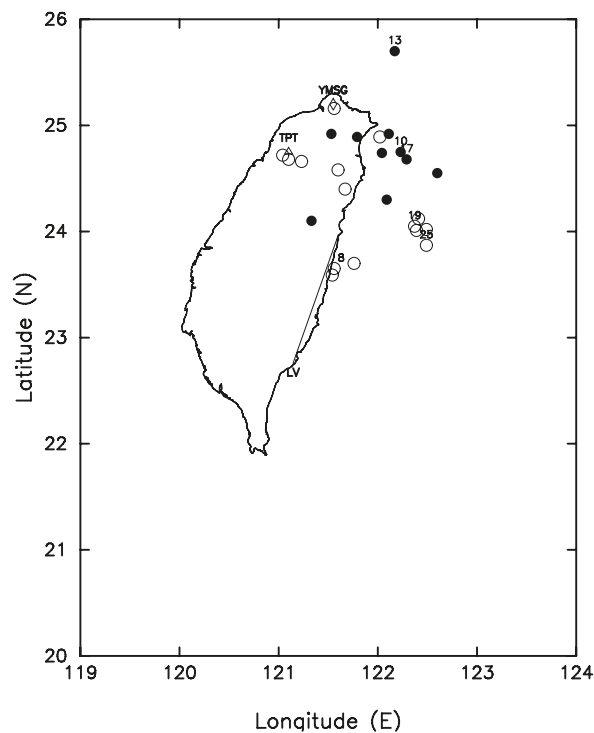


Figure 2. The figure shows the epicenters (open circles for $d \leq 40$ km and solid circles for $d > 40$ m) of the earthquakes as listed in Table 1. The radon monitoring station YMSG is shown by an open diamond symbol. The γ -ray monitoring station TPT is shown by an open triangle. A thin line marked with 'LV' in eastern Taiwan represents the Longitudinal Valley.

Fig. 2 (open circles for the events with $d \leq 40$ km and solid circle for those with $d > 40$ km). Clearly, only one event is located near the YMSG station, three events close to the TPT station, and others far away from the two stations with $\Delta > 40$ km. At stations YMSG and TPT, Fu et al. [2019] reported that the temporal variations of γ -ray and Rn have similar patterns. They also mentioned three interesting points. First, some high γ -ray and Rn concentration peaks in the entire spectrum. Secondly, the increase of γ -ray emission changes usually come after the Rn concentration anomalies as listed in Table 1. Thirdly, although the duration time of Rn concentration anomalies is longer than that of γ -ray emission changes, the two types of precursors disappeared almost at the same time before the forthcoming earthquake.

No	time	epicenter		M_L	d	Δ	T_{Rn}	T_{gr}	$T_{Rn} - T_{gr}$	Remarks
01	2014/07/26 00:43	122.11	24.92	4.0	101.0	61.0	0	4		
02	2014/08/01 12:38	121.60	24.58	4.0	6.1	64.0	0	3		
03	2014/08/05 08:34	121.67	24.40	3.6	38.0	84.0	0	3		
04	2014/08/16 02:51	121.53	24.92	3.8	84.0	26.0	0	7		
05	2014/08/17 06:52	121.04	24.72	2.3	6.2	71.0	3	0		
06	2014/08/24 20:39	122.09	24.30	4.0	57.5	109.0	0	6		
07	2014/09/21 05:14	121.54	23.59	5.0	31.5	173.0	21	0		
08	2014/10/08 02:08	121.56	23.65	5.2	33.4	167.0	15	10	5	ETeD*
09	2014/10/19 17:50	121.10	24.68	2.9	6.0	70.0	4	0		
10	2014/10/26 12:47	122.23	24.75	5.0	86.0	81.0	8	3	5	
11	2014/11/18 07:22	121.56	25.16	2.8	2.5	1.0	0	2		
12	2014/11/20 01:46	122.02	24.89	5.2	13.9	55.0	17	17(?)		
13	2014/12/11 05:03	122.17	25.70	6.7	268.6	86.0	23	14	9	
14	2014/12/31 11:06	121.79	24.89	5.1	68.9	37.0	0	20		
15	2014/12/31 15:54	122.60	24.55	5.6	96.1	125.0	0	20		
16	2015/01/05 13:53	122.04	24.74	5.1	73.8	67.0	0	20(?)		
17	2015/02/27 00:50	122.29	24.68	5.3	97.6	90.0	13	11	2	
18	2015/03/23 18:13	121.76	23.70	6.2	38.4	162.0	9	0		
19	2015/04/20 09:42	122.37	24.05	6.4	30.6	147.0	21	12	9	
20	2015/04/20 09:49	122.49	24.02	5.0	30.7	157.0	21(?)	12(?)		
21	2015/04/20 19:45	122.41	24.12	6.2	33.9	143.0	21(?)	12(?)		
22	2015/04/20 19:59	122.39	24.01	6.0	29.4	152.0	21(?)	12(?)		
23	2015/05/07 04:04	121.33	24.10	4.4	68.0	119.0	0	4		
24	2015/05/09 20:32	121.23	24.66	3.5	10.0	64.0	1	0		
25	2015/05/26 08:56	122.49	23.87	5.0	28.9	171.0	7	6	1	ETeD*

?: The values are questionable and thus the event is not in use.
 *: The event of the testing dataset

Table 1. The source parameters (date, epicenter, local magnitude, M_L , and focal depth, d) of the events for which the Rn concentration changes and the γ -ray emissions were observed by Fu et al. [2015; 2019]. The parameters T_{Rn} (in days) and T_{gr} (in days) denote the precursors times, respectively, for the Rn concentration changes and the γ -ray emissions before the related earthquake. Rn concentration anomalies were monitored at the YMSG station, while γ -ray emission changes were done at the TPT station.

Based on the data obtained by Fu et al. [2019], Wang [2021b] explored the correlation between the Rn concentration anomalies and γ -ray emission changes. He defined T_{Rn} (in days) and T_{gr} (in days) to be the precursor time of the former and that of the latter, respectively. From the plot of T_{gr} versus T_{Rn} , he found an increase in T_{gr} with T_{Rn} . From the plot of $T_{Rn}-T_{gr}$ versus T_{Rn} , he saw an increase in $T_{Rn}-T_{gr}$ with T_{Rn} even though the data points are somewhat scattered. Results reveal that the γ -ray emission change is associated with the Rn concentration anomaly as mentioned by Fu et al. [2019]. From the plot of T_{gr} and T_{Rn} versus M_L , Wang [2021b] found the increases in both T_{Rn} and T_{gr} with M_L , thus suggesting that the larger the forthcoming earthquake is, the earlier the occurrence times of the two precursors are. From the plot of $T_{Rn}-T_{gr}$ versus M_L , he also saw an increase in $T_{Rn}-T_{gr}$ with M_L . This suggests that when the occurrence time of γ -ray emission change after the Rn concentration anomaly is longer, the forthcoming earthquake is bigger and its occurrence time is longer after the appearance of the two types of precursors. Based on the above-mentioned physical theory, we may predict the forthcoming mainshocks by using the observed $\log(T)-M$ relationships of Rn concentration anomalies and γ -ray emission changes.

In the followings, the regression equations of precursor time versus local magnitude are inferred on the basis of the least square estimation [cf. Press et al., 1986]. In order to perform the least square estimation of the $\log(T)-M_L$ relationship, we need to establish a ‘training dataset.’ Meanwhile, we also need a ‘testing dataset’ to examine the model with related parameters for evaluating the magnitude and failure time of a forthcoming earthquake. As listed in Table 1, the γ -ray emission changes were recorded before 20 events. First, two events, i.e., Event 08 and Event 25, are taken as the testing events to form the testing dataset not only for the γ -ray emission changes but also for the Rn concentration anomalies and. Clearly, $T_{gr} = T_{Rn} = 17$ days for Event 12 is questionable for the γ -ray emission changes. Event 16 could be the largest aftershock of Event 15, and thus it must be deleted. Event 20, 21, and 22 could be the aftershocks of Event 19, and thus they must be removed. Excluding the 7 events, 14 events are taken to form the training dataset for the γ -ray emission changes.

The plots of T_{gr} versus M_L and $\log(T_{gr})$ versus M_L for the 14 events with T_{gr} are displayed in Figure 3a and Figure 3b, respectively. From the data points, the inferred regression equations of $\log(T_{gr})$ versus M_L is

$$\log(T_{gr}) = (-0.29 \pm 0.23) + (0.24 \pm 0.02)M_L. \quad (16)$$

Equation (16) is displayed with a thin solid line in Fig. 3.

As listed in Table 1, the Rn concentration anomalies were recorded before 15 events. Clearly Events 20, 21, and 22 are the aftershocks of Event 19, and thus they must be removed. Excluding the 3 events and 2 events of the testing dataset, there are 9 events in the training dataset for Rn concentration changes. The plots of T_{Rn} versus M_L and $\log(T_{Rn})$ versus M_L for the 9 events with T_{Rn} are displayed in Figure 4a and Figure 4b, respectively. From the data points as shown in the figure, the inferred regression equations of $\log(T_{Rn})$ versus M_L is

$$\log(T_{Rn}) = (-0.21 \pm 0.30) + (0.23 \pm 0.02)M_L \quad (17)$$

Equation (17) is displayed with a thin solid line in Fig. 4.

For 111 earthquakes, Liu et al. [1984], Chyi et al. [2001, 2005], Yang et al. [2005], Fu et al. [2017a, 2017b, 2017c, 2019], and Kuo et al. [2006a,b, 2010, 2017, 2018, 2019, 2020] observed the Rn concentration changes before these events on several automatically monitoring stations in Taiwan. The plots of T_{Rn} versus M_L and $\log(T_{Rn})$ versus M_L are displayed in Figure 5a and Figure 5b, respectively.

In Fig. 5, the open and solid circles are made, respectively, for the events with $d \leq 40$ km and $\Delta \leq 40$ km and for those with $d > 40$ km and $\Delta > 40$ km. From these data, Wang [2021b] inferred the $\log(T_{Rn})-M_L$ relationships as:

$$\log(T_{Rn}) = (-2.05 \pm 0.40) + (0.58 \pm 0.01)M_L \quad (18)$$

for the events with $d \leq 40$ km and $\Delta \leq 40$ km and

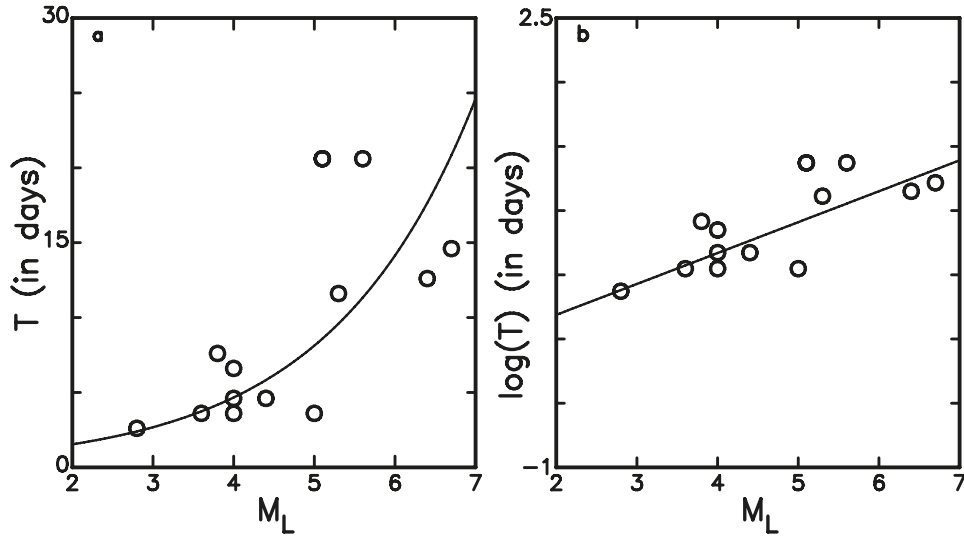


Figure 3. (a) Plot of T versus M_L and (b) plot of $\log(T)$ versus M_L for γ -ray emission changes for 15 events that are explained in the text and listed in Table 1. The thin solid line represents Equation (16) listed in the text.

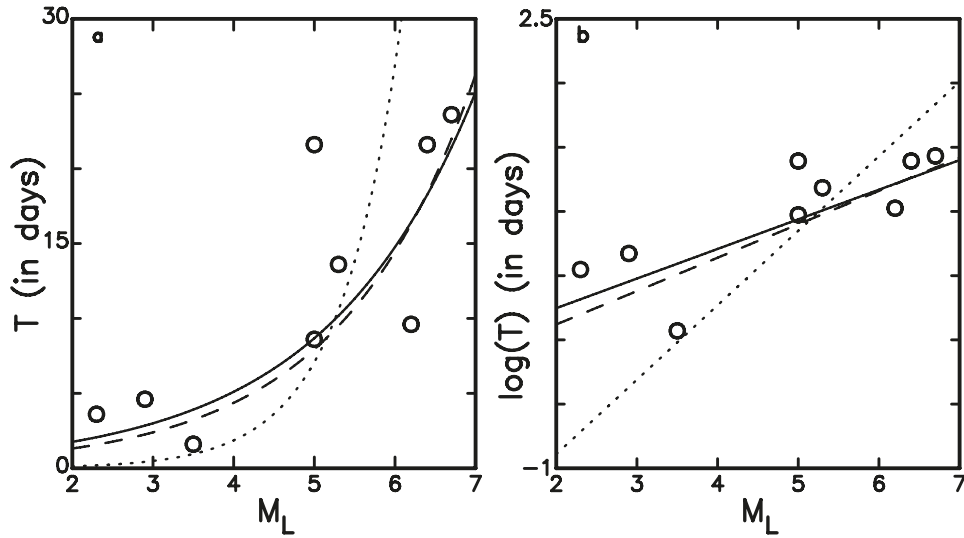


Figure 4. (a) Plot of T versus M_L and (b) plot of $\log(T)$ versus M_L for Rn concentration anomalies for 12 events that are explained in the text and listed in Table 1. The solid line represents Equation (17) listed in the text. The dashed line and dotted line represent, respectively, Equation (18) and Equation (19) listed in the text.

$$\log(T_{Rn}) = (-0.40 \pm 0.42) + (0.26 \pm 0.01)M_L \quad (19)$$

for those with $d > 40$ km or $\Delta > 40$ km. Equations (18) and (19) are displayed with a dashed line and a dotted line, respectively, in Fig. 5 and also in Fig. 4. In Fig. 4, the dashed line is in parallel with and close to the thin solid line, thus indicating that Equation (18) could be almost an average $\log(T_{Rn})-M_L$ relationship for Taiwan's earthquakes with $d \leq 40$ km and $\Delta \leq 40$ km. On the other hand, the dotted line is across the thin solid line with a large intersection angle. This means that Equation (19) cannot be the average $\log(T_{Rn})-M_L$ relationship for Taiwan's earthquakes with $d > 40$ km or $\Delta > 40$ km.

In order to solve M_L from Equations (16) and (17) based on the physical basis as shown in Equation (13), the observed Rn concentration anomalies and γ -ray emission changes are, respectively, considered as the first and second precursors. Hence, we have $a_1 = -0.21$, $b_1 = 0.23$, $a_2 = -0.29$, and $b_2 = 0.24$. This exhibits the second condition

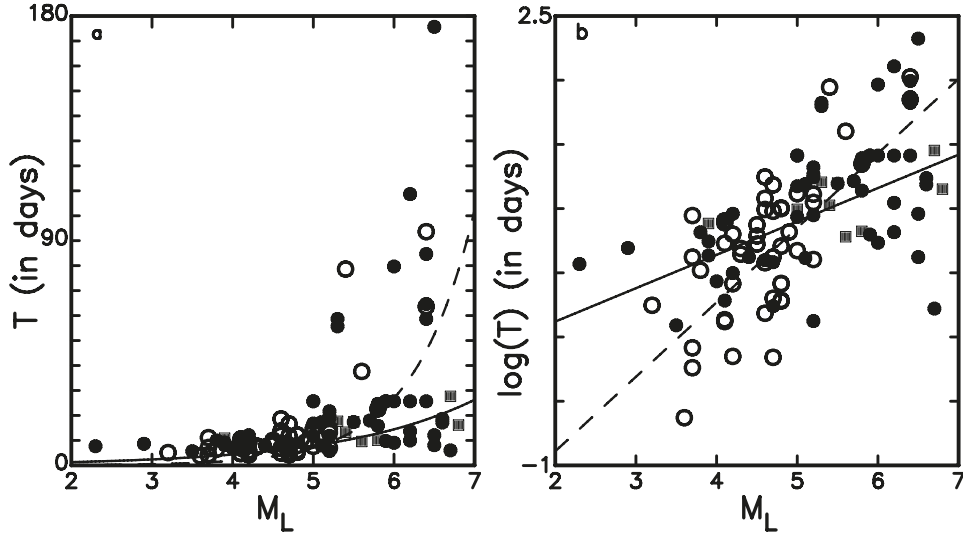


Figure 5. (a) Plot of T versus M_L and (b) plot of $\log(T)$ versus M_L for Rn concentration anomalies (open circles for the events with $d \leq 40$ km and $\Delta \leq 40$ km and solid circles for those with $d > 40$ km and $\Delta > 40$ km). The dashed line and thin solid line represent, respectively, Equation (18) and Equation (19) listed in the text.

with $a_1 > a_2$ and $b_1 \leq b_2$. Hence, M_L may be solved from Equation (13). From the third requirement as mentioned in Section 3, we must also take the standard deviations δa_i and δb_i of a_i and b_i , respectively, into account. The values are $\delta a_1 = 0.30$ and $\delta b_1 = 0.02$ for $F_1(M_L)$ from Equation (17) and $\delta a_2 = 0.29$ and $\delta b_2 = 0.02$ for $F_2(M_L)$ from Equation (19). Hence, we have $F_1(M_L) = t_{Rn} + 10^{(-0.21 \pm 0.30) + (0.23 \pm 0.02)M_L}$ and $F_2(M_L) = t_{gr} + 10^{(-0.29 \pm 0.25) + (0.24 \pm 0.02)M_L}$ where t_{Rn} and t_{gr} are the occurrence times of Rn concentration anomalies and γ -ray emission changes, respectively. Based on Equations (11) and (12), the values of $F_1(M_L)$ and $F_2(M_L)$ are both equal to t_r . Considering $t_{Rn} = 0$ as the initial time for each event for convenience, the value of t_{gr} is thus $\delta T = T_{Rn} - T_{gr}$. This means that when the difference in occurrence times between two different precursors have been measured, we may evaluate the magnitude and also the failure time of a forthcoming earthquake based on the $\log(T)$ - M_L relationships.

In order to include the effects of standard deviations, we will solve M_L through an alternative way. We define three difference functions of $F_2(M_L) - F_1(M_L)$: $\delta F_0(M_L) = \delta T + 10^{(-0.29 + 0.24M_L)} - 10^{(-0.21 + 0.23M_L)}$ without the standard deviations; $\delta F_{lb}(M_L) = \delta T + 10^{(-0.54 + 0.22M_L)} - 10^{(-0.51 + 0.21M_L)}$ with the negative standard deviations; and $\delta F_{ub}(M_L) = \delta T + 10^{(-0.04 + 0.26M_L)} - 10^{(+0.09 + 0.25M_L)}$ with the positive standard deviations. Clearly, $\delta F_{lb}(M_L)$ and $\delta F_{ub}(M_L)$ are, respectively, the lower-bound (denoted by ‘lb’) and upper-bound (denoted by ‘ub’) values of $\delta F_0(M_L)$ at a certain M_L .

As shown in Figure 6, the lb curve for $(a - \delta a) + (b - \delta b)M$ and the ub curve for $(a + \delta a) + (b + \delta b)M$ are both illustrated by dashed lines. A vertical dotted line segment denoted by ‘ T_{ub} ’ at the upper end and by ‘ T_{lb} ’ at the lower end exhibits the range of estimated values of T at a certain M . Hence, the ub and lb curves show the ub and lb values, respectively, for T . On the other hand, a horizontal dotted line segment denoted by ‘ M_{ub} ’ at the right end and by ‘ M_{lb} ’ at the left end exhibits the range of estimated values of M at a certain T . Hence, the ub and lb curves exhibit the lb and ub values, respectively, for M .

Note that for the purpose of reference, the magnitudes of Events 10, 13, 17, and 19 in the training dataset are also evaluated from the above-mentioned method. The six events are displayed in Fig. 2 with event number. We calculate the values of $\delta F_0(M_L)$, $\delta F_{lb}(M_L)$, and $\delta F_{ub}(M_L)$ from $M_L = 0$ to $M_L = 10$ for the six events. Results are plotted in Figure 7 in which $\delta F_{lb}(M_L)$, $\delta F_0(M_L)$ and $\delta F_{ub}(M_L)$ are normalized by the maximum value of either $|\delta F_{lb}(M_L)|$ or $|\delta F_{ub}(M_L)|$ in each panel for the related event. The three difference functions are illustrated by different curves: a thin solid line for $\delta F_0(M_L)$, a thin dashed line for $\delta F_{lb}(M_L)$, and a thin dotted line for $\delta F_{ub}(M_L)$. In each panel of Fig. 7, a horizontal solid line represents $F_2(M_L) - F_1(M_L) = 0$ and a vertical solid line denotes the observed value of M_L of the related event as listed in Table 1. If the curve of $F_2(M_L) - F_1(M_L)$ intersects with the horizontal solid line at a certain point, we may evaluate the value of M_L at the intersection point. The expected, lower-bound, and upper-bound values of M_L are denoted by M_{L0} , M_{Llb} (related to M_{lb} in Fig. 6), and M_{Lub} (related to M_{ub} in Fig. 6), respectively, and they are evaluated from $\delta F_0(M_L) = 0$, $\delta F_{ub}(M_L) = 0$, and $\delta F_{lb}(M_L) = 0$, respectively.

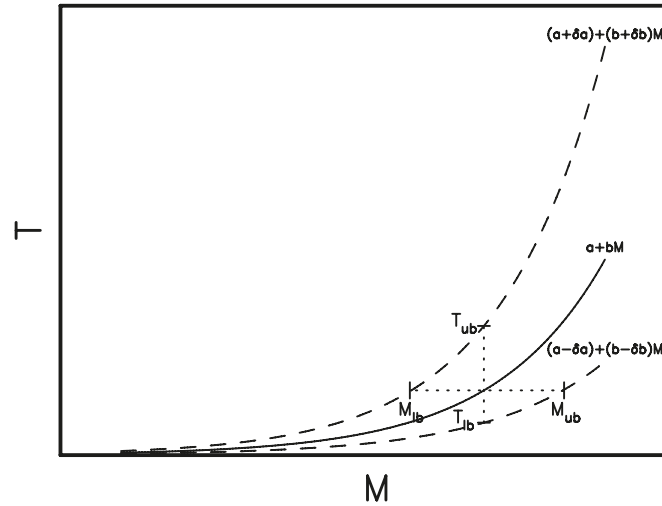


Figure 6. Plot of T versus M : the solid line for $a + bM$; the lower dashed line for $(a - \delta a) + (b - \delta b)M$; and the upper dashed line for $(a + \delta a) + (b + \delta b)M$. A vertical dotted line segment denoted by ' T_{ub} ' at the upper end and by ' T_{lb} ' at the lower end exhibits the range of estimated values of T at a certain M . A horizontal dotted line segment denoted by ' M_{ub} ' at the right end and ' M_{lb} ' at the left end exhibits the range of estimated values of M .

Figure 7 shows that the thin dashed line for $\delta F_{lb}(M_L)$ and the thin dashed line for $\delta F_0(M_L)$ both only increase with M_L from $M_L = 0$ to $M_L = 10$, but they do not intersect the horizontal line at a point. Hence, we cannot estimate the values of M_{Lub} and M_{L0} . The thin dotted line for $\delta F_{ub}(M_L)$ decreases with increasing M_L from $M_L = 0$ to $M_L = 10$ and intersects the horizontal line at a point with M_{Lib} . Hence, we can estimate the values of M_{Lib} for the six events. The estimated values of M_{Lib} and M_{L0} for the six events are listed in Table 2. Figure 7 and Table 2 show that M_{Lib} is

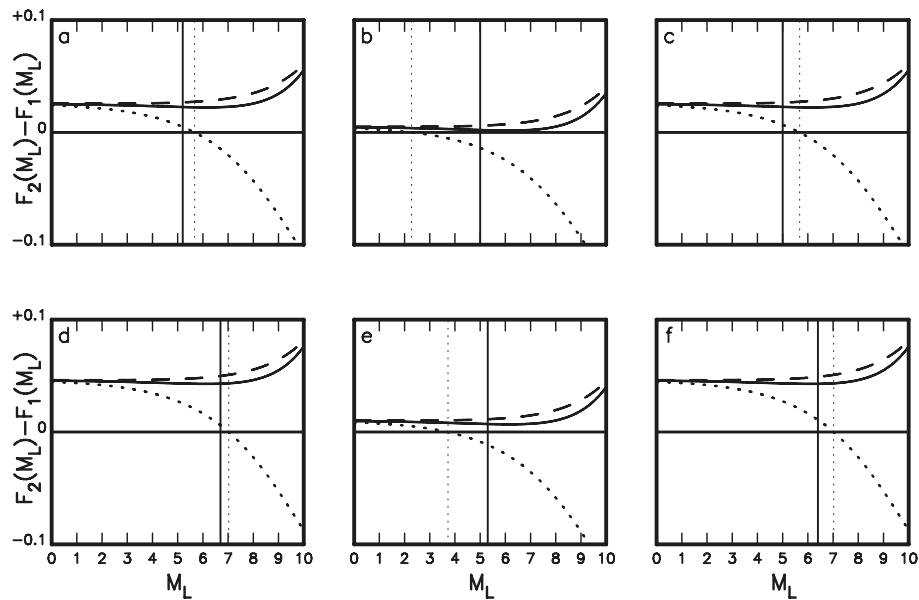


Figure 7. The curves of for the differences between normalized $F_2(M_L)$ (for γ -ray emission changes) and normalized $F_1(M_L)$ (for Rn concentration anomalies) based on Equation (17): (a) for event 08 with $M_L = 5.2$; (b) for event 25 with $M_L = 5.0$; (c) for event 10 with $M_L = 5.0$; (d) for event 13 with $M_L = 6.7$; (e) for event 17 with $M_L = 5.3$; and (f) for event 19 with M_L . In each panel, the solid, dotted, and dashed curves represent the $\delta F(M_L)$, $\delta F_{lb}(M_L)$, and $\delta F_{ub}(M_L)$, respectively. The vertical line denotes the observed value of M_L for each event; the vertical thin solid line for the estimated value of M_{L0} and the vertical thin dotted line for the estimated value of M_{Lib} . The estimated values of M_{L0} and M_{Lib} are listed in Table 2.

larger and smaller than observed M_L for Event 08 and Event 25, respectively, and M_{Llb} is smaller than observed M_L for Event 17 and larger than observed M_L for Events 10, 17, and 199. The values of $M_L - M_{Llb}$ vary from -0.33 to +2.72.

We also evaluate the values of M_{L0} , M_{Llb} , and M_{Lub} , from Equation (16) plus Equation (19). The coefficients are $a_1 = -0.40$, $b_1 = 0.26$, $a_2 = -0.29$, and $b_2 = 0.24$. This exhibits the first condition with $a_1 < a_2$ and $b_1 > b_2$. Hence, M_L may be solved from Equation (13). The values of standard deviations are: $\delta a_1 = 0.02$ and $\delta b_1 = 0.01$ for $F_1(M_L)$ from Equation (19) and $\delta a_2 = 0.25$ and $\delta b_2 = 0.02$ for $F_2(M_L)$ from Equation (16). The three difference functions of $F_2(M_L) - F_1(M_L)$ are: $\delta F_0(M_L) = \delta T + 10^{(-0.29 + 0.24ML)} - 10^{(-0.40 + 0.26ML)}$, $\delta F_{lb}(M_L) = \delta T + 10^{(-0.54 + 0.22ML)} - 10^{(-0.82 + 0.25ML)}$, and $\delta F_{ub}(M_L) = \delta T + 10^{(-0.04 + 0.26ML)} - 10^{(+0.02 + 0.27ML)}$.

Event No. (M_L)	M_{Llb} and M_{L0} from Equations (16) and (17)	$M_L - M_{Llb}$ from Equations (16) and (17)	M_{Llb} , M_{L0} , and M_{Lub} from Equations (16) and (19)	$M_L - M_{Llb}$ and $M_{L0} - M_L$ from Equations (16) and (19)
08 (5.2)	5.68, -	-0.42	4.93, 7.98, -	+0.27, +2.78
25 (5.0)	2.28, -	+2.72	2.68, 6.57, 9.68	+2.32, +1.57
10 (5.0)	5.68, -	-0.68	4.93, 7.98, -	+0.07, +2.98
13 (6.7)	7.03, -	-0.33	5.78, 8.58, -	+0.92, +1.88
17 (5.3)	3.72, -	+1.58	3.62, 7.12, 9.98	+1.68, +1.82
19 (6.4)	7.03, -	-0.63	5.78, 8.58, -	+0.62, +2.18

Table 2. The number and M_L for the six events in consideration, the estimated values of M_{Llb} and M_{L0} from Equations (16) and (17) and those from Equations (16) and (19).

We calculate the values of three functions of differences between $F_2(M_L)$ and $F_1(M_L)$ from $M_L = 0$ to $M_L = 10$ for the above-mentioned six events, i.e., Events 08 and 25 in the testing dataset and Events 10, 13, 17, and 19 in the training dataset. Results are plotted in Figure 8 in which $\delta F_{lb}(M_L)$, $\delta F_0(M_L)$, and $\delta F_{ub}(M_L)$ are normalized by the maximum value of either $|\delta F_{lb}(M_L)|$ or $|\delta F_{ub}(M_L)|$ for each event. The three difference functions are shown with different curves: a thin solid line for $\delta F_0(M_L)$, a thin dashed line for $\delta F_{lb}(M_L)$, and a thin dotted line for $\delta F_{ub}(M_L)$. In each panel of Fig. 8, a horizontal line represents $F_2(M_L) - F_1(M_L) = 0$ and a vertical solid line denotes the observed value of M_L of the related event. Figure 8 shows that the thin dashed line for $\delta F_{ub}(M_L)$ increases and then decreases with increasing M_L from $M_L = 0$ to $M_L = 10$ and does not intersect the horizontal line at a point for Events 08, 10, 13, and 19 and intersects the horizontal line at a point for Events 25 and 19. Hence, we can estimate the value of M_{Lub} for the latter two events. The thin solid line for $\delta F_0(M_L)$ and the thin dotted line for $\delta F_{lb}(M_L)$ both decrease with increasing M_L from $M_L = 0$ to $M_L = 10$ and intersect the horizontal line at respective points. Hence, we can estimate the values of M_{L0} and M_{Llb} for the six events. The values of M_{Llb} , M_{L0} , and M_{Lub} for the six events are listed in Table 2.

Table 2 reveals that from Equation (16) plus Equation (19), M_{Llb} are all smaller than observed M_L and M_{L0} are all larger than observed M_L for the six events. The values of $M_L - M_{Llb}$ and $M_{L0} - M_L$ are 0.07-2.32 and 1.57-2.98, respectively. Hence, observed M_L is in between M_{Llb} and M_{L0} for the six events. This seems to suggest that it is better to use Equation (16) plus Equation (19) than to use Equation (16) plus Equation (17) to evaluate the value of M_L for a forthcoming earthquake. This is due to a reason that the number of training dataset for Rn concentration changes from the observations made in a local area is much smaller than that done in a large region.

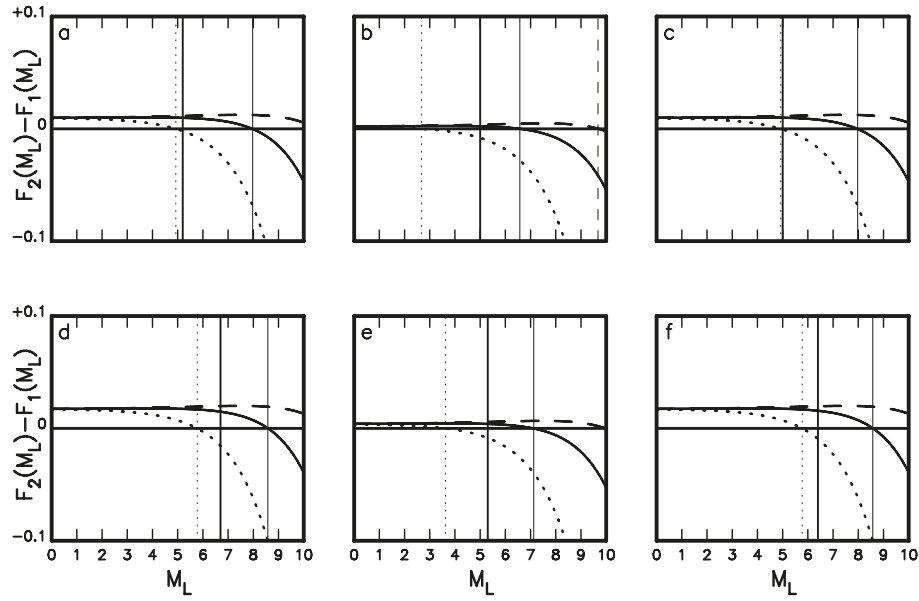


Figure 8. The curves of for the differences between normalized $F_2(M_L)$ (for γ -ray emission changes) and normalized $F_1(M_L)$ (for Rn concentration anomalies) based on Equation (19): (a) for event 08 with $M_L = 5.2$; (b) for event 25 with $M_L = 5.0$; (c) for event 10 with $M_L = 5.0$; (d) for event 13 with $M_L = 6.7$; (e) for event 17 with $M_L = 5.3$; and (f) for event 19 with M_L . In each panel, the thin solid, dotted, and dashed curves represent the $\delta F(M_L)$, $\delta F_{ub}(M_L)$, and $\delta F_{lb}(M_L)$, respectively. The vertical line denotes the observed value of M_L for each event; the vertical thin solid line for the estimated value of M_{L0} and the vertical thin dotted line for the estimated value of M_{Llb} . The estimated values of M_{L0} and M_{Llb} are listed in Table 2.

4.2 Evaluation of the Precursor Time of Rn Concentration Anomalies

We may evaluate the precursor times for both Rn concentration anomalies and γ -ray emission changes from the evaluated value of M_L , i.e., M_{L0} . Here, only the former is taken into account. The expected, lower-bound, and upper-bound values of precursor time are denoted by T_{Rn0} , T_{Rnlb} (related to T_{lb} in Fig. 6), and T_{Rnub} (related to T_{ub} in Fig. 6) are evaluated based on the value of M_{L0} . From Equation (16) plus Equation (17), the three quantities are computed from the following equations: $T_{Rn0}(M_{L0}) = 10^{(-0.21 + 0.23M_{L0})}$, $T_{Rnlb}(M_{L0}) = 10^{(-0.51 + 0.21M_{L0})}$, and $T_{Rnub}(M_{L0}) = 10^{(0.09 + 0.25M_{L0})}$. From Equation (16) plus Equation (19), the three quantities are computed from the following equations: $T_{Rn0}(M_{L0}) = 10^{(-0.40 + 0.26M_{L0})}$, $T_{Rnlb}(M_{L0}) = 10^{(-0.82 + 0.25M_{L0})}$, and $T_{Rnub}(M_{L0}) = 10^{(0.02 + 0.27M_{L0})}$. For the 6 events, the values of T_{Rnlb} , T_{Rn0} , and T_{Rnub} computed from the two ways are listed in Table 3. Note that from the observed data, the failure time, t_r , of the forthcoming earthquake will be $t_r = t_{Rn} + T_{Rn}$.

Table 3 reveals that from Equation (16) plus Equation (17), only T_{Rnlb} can be evaluated for the six events, yet not for T_{Rn0} because the value of M_{L0} is unknown. Observed T_{Rn} is longer than T_{Rnlb} for Events 25 and 19 and shorter than T_{Rnlb} for Events 8, 10, 13, and 17. The value of $T_{Rn0} - T_{Rnlb}$ ranges from -62.2 days to +10.5 days. From Equation (16) plus Equation (19), T_{Rnlb} and T_{Rn0} can be evaluated for the six events because the values of M_{Llb} and M_{L0} have been evaluated and T_{Rnub} can be estimated for Events 25 and 17 because their values of M_{Llb} are known. Results show that observed T_{Rn} is longer than T_{Rnlb} for Events 25, 13, and 17 and shorter than T_{Rnlb} for Events 8, 10, and 19. The value of $T_{Rn0} - T_{Rnlb}$ ranges from -30.0 days to 3.0 days. For the six events, observed T_{Rn} is shorter than T_{Rn0} and thus the value of $T_{Rn0} - T_{Rn}$ ranges from 13.4 days to 59.5 days. In other word, observed T_{Rn} is in between T_{Rnlb} and T_{Rn0} only for Events 25, 13, and 17 and not for the others. The value of $T_{Rnub} - T_{Rn}$ are 32.7 days and 34.2 days, respectively, for Event 25 and Event 17.

Event No. (T_{Rn})	T_{Rnlb} and T_{Rn0} from Equations (16) and (17)	$T_{Rn}-T_{Rnlb}$ from Equations (16) and (17)	T_{Rnlb} , T_{Rn0} , and T_{Rnub} from Equations (16) and (19)	$T_{Rn}-T_{Rnlb}$ and $T_{Rn0}-T_{Rn}$ from Equations (16) and (19)
08 (15)	32.2, –	–17.2	22.4, 47.2, –	–7.4, +32.2
25 (7)	4.6, –	+2.4	5.5, 20.4, 39.7	+1.5, +13.4
10 (8)	70.2, –	–62.2	38.0, 67.5, –	–30.0, +59.5
13 (23)	32.3, –	–9.3	22.4, 47.2, –	+0.6, +24.2
17 (13)	70.2, –	–57.2	10.0, 28.3, 47.2	+3.0, +15.3
19 (21)	10.5, –	+10.5	38.0, 67.5, –	–18.0, +46.5

Table 3. The number and T_{Rn} (in days) for the six events in consideration, the estimated values of T_{Rnlb} , T_{Rn0} , and T_{Rnub} from Equations (16) and (17) and those from Equations (16) and (19).

4.3 Discussion

In principle, we expect that it is better to evaluate the values of M_L and T_{Rn} from the $\log(T)-M_L$ relationships inferred from the data observed in a local area than from those done from the data observed in a large region, for example, the whole Taiwan region. But, Fig. 7 shows that the curves of $\delta F_0(M_L)$ and $\delta F_{ub}(M_L)$ do not intersect the horizontal solid line with $F_2(M_L)-F_1(M_L) = 0$ at a certain point. This make us be unable to estimate the values of M_{L0} and M_{Lub} that are the expected and upper-bound values of M_L , respectively. This indicates that the magnitude of the forthcoming earthquake may not be estimated in a reasonable range when the number of training dataset for the Rn concentration changes obtained from a local area is not large enough for inferring an acceptable $\log(T)-M_L$ relationship. On the other hand, when the Rn concentration anomalies are observed in a large region, the number of training dataset is large enough for inferring a reliable $\log(T)-M_L$ relationship. This will lead to reliable and acceptable evaluations of the magnitude and failure time of a forthcoming earthquake. Clearly, the $\log(T)-M_L$ relationship inferred from the γ -ray emission changes seems good, even though the number of training dataset is only 14. Of course, its standard deviations are somewhat high and need improvement from more accurate data. Consequently, we assume that a single dataset consisting of a large number of same earthquakes having the observed values of both T_{gr} and T_{Rn} will substantially improve the evaluated vales of M_L and T_{Rn} .

The γ -ray emission is mainly produced from the radioactive decay of Rn [e.g., Tsukuda, 2008; Minnehan, 2015]. ^{222}Rn first decays, with a half time of 3.8 days, to ^{218}Po . During the decaying processes, there are α -particle (^4He) emissions with energy release of 5.49 MeV and energy release by γ -ray emissions. Hence, the value of δT should be 3.8 days when the two precursors are observed at the same site. Although the two precursors were observed at two different sites, it is still necessary to further explore the reason why δT is shorter than 3 days for Events 17 and 25.

Tables 2 and 3 seem to suggest that it is more reliable to evaluate the magnitude than to estimate the failure time for a forthcoming earthquake based on the given $\log(T)-M_L$ relationships. This might be due to a fact that in the relationship, the precursor time and the magnitude are represented, respectively, by $\log(T)$ and M_L . Hence, the high standard deviations, especially for a_i ($i = 1$ and 2), of the $\log(T)-M_L$ relationships will yield a remarkable difference in evaluations between T and M_L . High standard deviations will yield larger uncertainty of evaluated value of T_{Rn} than that of M_L . A reduction in the standard deviations from a larger number of reliable data will more substantially improve the evaluated vales of both M_L and T_{Rn} . This means that we should pay attention to

the accuracy of observations. Moreover, from the previous discussion we assume that more observations for Rn concentration changes and also for γ -ray emission changes in the local study area should be made in the future.

Usually, there are three basic and important parameters for prediction of a forthcoming earthquake, i.e., failure time, magnitude, and location. Clearly, there is a weak point about the present method. The source area where the forthcoming earthquake will happen cannot be predicted from the present method. It needs other precursors, for example, crustal deformation pattern, B -value anomalies, foreshock activities, electromagnetic anomalies etc., or other methods for predicting the possible source area of the forthcoming earthquake. For example, Hayakawa and Hobara [2010] described the goniometric method to detect the directions of ULF emissions from the observational stations to the earthquake epicenter and then to infer the possible location of the forthcoming event. This sounds a good way.

5. Conclusions

Observations of precursor time, T , of a certain kind of precursor and the magnitude, M , of the forthcoming earthquake lead to a relationship of $\log(T) = a + bM$. Based on the $\log(T)$ - M relationships of two different precursors from observed data, we propose a new method of predicting the magnitude and failure time of a forthcoming earthquake. First, we have explored the intrinsic physics of the $\log(T)$ - M relationship. Its physical basis is that there are power-law relations between T and the following three physical parameters: the linear dimension of source area, L , the strain energy, ΔE , and the Benioff strain of the forthcoming earthquake.

Secondly, we have studied the conditions and requirements on the $\log(T)$ - M relationships of two kinds of precursors which are taken for predicting the values of M and T for a forthcoming earthquake. Let a_i and b_i are the coefficients of the relationship for the i -th precursor. The first precursor appeared earlier than the second one. Theoretical analyses reveal that the value of M of a forthcoming mainshock may be solved under two conditions: (1) $a_1 < a_2$ and $b_1 > b_2$ and (2) $a_1 > a_2$ and $b_1 \leq b_2$.

Thirdly, we have given a testing example based on the relationships of $\log(T)$ versus M_L (M_L = local magnitude) for preseismic Rn concentration anomalies and gamma-ray emission changes that were observed on respective monitoring stations in Taiwan. The precursor times are T_{Rn} for Rn concentration anomalies and T_{gr} for γ -ray emission changes. The relationships are inferred through the least square estimation. The two relationships make us be able to evaluate M_L and T_{Rn} of a forthcoming earthquake. The failure time of the forthcoming earthquake is $t_r = t_{Rn} + T_{Rn}$ in which t_{Rn} is the occurrence time of Rn concentration anomalies. The standard deviations of the coefficients of the $\log(T)$ - M_L relationships can influence the evaluations of M_L and T_{Rn} . To reduce the standard deviations, especially for a_i ($i = 1$ and 2), from a large number of reliable data will substantially improve the evaluated values of M_L and T_{Rn} (as well as t_r). In addition, we assume that it will be much useful and reliable when the $\log(T)$ - M_L relationships for two different precursors are inferred from a dataset consisting of the same events.

Consequently, results confirm a high opportunity and feasibility of reliably predicting the magnitude and failure time of a forthcoming earthquake based on the observations of precursor times of the pairs of two different precursors.

Acknowledgments. I would like to express my deep thanks to two anonymous reviewers and Guest Editor Prof. Stelios M. Potirakis for their valuable comments and suggestions that help me to substantially improve the manuscript. The study was financially partly supported by Institute of Earth Sciences, Academia Sinica, Taiwan.

References

- Aggarwal, Y.P., L.R. Sykes, J. Armbruster and M.I. Sbar (1973). Premonitory changes in seismic velocities and prediction of earthquakes, *Nature*, 241, 101-104. doi:10.1038/241101a0.
- Aki, K. (1966). Generation and propagation of G waves from the Niigata earthquake of June 16, 1964. Part 2: Estimation of earthquake moment, from the G wave spectrum, *Bull. Earthquake Res. Inst., Tokyo Univ., Japan*, 44, 73-88
- Aki, K. (1967). Scaling law of seismic spectrum, *J. Geophys. Res.*, 72, 1217-1231.
- Aki, K. (1989). Ideal probabilistic earthquake prediction, *Tectonophysics*, 169, 197-198, doi:10.1016/0040-1951(89)90193-5.

- Aki, K. (2009). *Seismology of Earthquake and Volcano Prediction*, Science Press Beijing, China, 331. (with Chinese translation)
- Anderson, D.L. and J.H. Whitcomb (1975). Time-dependent seismology, *J. Geophys. Res.*, 80, 11, 1497-1503.
- Atkinson, R.K. (1984). Subcritical crack growth in geological materials, *J. Geophys. Res.*, 89, 4077-4114.
- Bufe, C.G. and D.J. Varnes (1993). Predictive modeling of the seismic cycle of the greater San Francisco Bay region. *J. Geophys. Res.*, 98, B6, 9871-9883.
- Chyi, L.L., C.Y. Chou, F.T. Yang and C.H. Chen (2001). Continuous radon measurements in faults and earthquake precursor pattern recognition, *Western Pacific Earth Sci.*, 1, 2, 43-72.
- Chyi, L.L., T.J. Quick, F.T. Yang and C.H. Chen (2005). Soil gas radon spectra and earthquakes, *Terr. Atmos. Ocean. Sci.*, 16, 763-774.
- Dieterich, J.H. (1978). Preseismic fault slip and earthquake prediction, *J. Geophys. Res.*, 83, B8, 3940-3948.
- Ding, G., T. Ma and S. Ma (1985). Methods of earthquake prediction. in F.F. Evison (Editor), *Earthquake Prediction*, Terra Scientific Publishing Co., Tokyo, Unesco, Paris, 453-465.
- Enomoto, Y. (2012). Coupled interaction of earthquake nucleation with deep Earth gases: a possible mechanism for seismo-electromagnetic phenomena, *Geophys. J. Intl.*, 191, 1210-1214.
- Field, E.H. (2019). How physics-based earthquake simulators might help improve earthquake forecasts, *Seism. Res. Lett.*, 90, 2A, 467-472, doi:10.1785/0220180299.
- Frid, V. and K. Vozoff (2005). Electromagnetic radiation induced by mining rock failure, *Int. J. Coal Geol.*, 64, 57-65.
- Frid, V., J. Goldbaumb, A. Rabinovitchc and D. Baha (2011). Time-dependent Benioff strain release diagrams, *Philosophical Magazine*, 91, 12, 1693-1704.
- Fu, C.C., P.K. Wang, L.C. Lee, C.H. Lin, W.Y. Chang, G. Giuliani and D. Ouzounov (2015). Temporal variation of gamma rays as a possible precursor of earthquake in the Longitudinal Valley of eastern Taiwan, *J. Asian Earth Sci.*, 114, 2, 362-372.
- Fu, C.C., T.F. Yang, C.H. Chen, L.C. Lee, Y.M. Wu, T.K. Liu, V. Walia, A. Kumar and T.H. Lai (2017a). Spatial and temporal anomalies of soil gas in northern Taiwan and its tectonic and seismic implications, *J. Asian Earth Sci.*, 149, 64-77.
- Fu, C.C., T.F. Yang, M.C. Tsai, L.C. Lee, T.K. Liu, V. Walia, C.H. Chen, W.Y. Chang, A. Kumar and T.H. Lai (2017b). Exploring the relationship between soil degassing and seismic activity by continuous radon monitoring in the Longitudinal Valley of eastern Taiwan, *Chem. Geol.*, 469, 163-175.
- Fu, C.C., V. Walia, T.F. Yang, L.C. Lee, T.K. Liu, C.H. Chen, A. Kumar, T.H. Lai and K.L. Wen (2017c). Preseismic anomalies in soil-gas radon associated with 2016 M6.6 Meinong earthquake, Southern Taiwan, *Terr. Atmos. Ocean. Sci.*, 28, 5, 787-798.
- Fu, C.C., L.C. Lee, T.F. Yang, C.H. Lin, C.H., Chen, V. Walia, T.K. Liu, D. Ouzounov, G. Giuliani, T.H. Lai and P.K. Wang (2019). Gamma ray and radon anomalies in Northern Taiwan as a possible pre-earthquake indicator around the plate boundary, *Geofluids*, 2019, Article ID 4734513, 14, doi:10.1155/2019/4734513.
- Geller, R.J. (1996). Special issue: Debate on "VAN", *Geophys. Res. Letts*, 23, 11, 1291-1293.
- Geller, R.J. (1997). Earthquake prediction: a critical review, *Geophys. J. R. Astro. Soc.*, 131, 425-450.
- Geller, R.J., D.D. Jackson, Y.Y. Kagan and F. Mulargia, (1997). Earthquakes cannot be predicted, *Science*, 275, 536, 1616-1617, doi:10.1126/science.275.5306.1616.
- Gutenberg, B. and C.F. Richter (1942). Earthquake magnitude, intensity, energy and acceleration, *Bull. Seism. Soc. Am.*, 32, 163-191.
- Gutenberg, B. and C.F. Richter (1944). Frequency of earthquakes in California, *Bull. Seism. Soc. Am.*, 34, 185-188.
- Gutenberg, B. and C.F. Richter (1956). Magnitude and energy of earthquake, *Annali di Geofisica*, 9, 1-15.
- Hayakawa, M. and Y. Hobara (2010). Current status of seismo-electromagnetic for short-term earthquake prediction, *Geomatics, Natural Hazards and Risk*, 1, 2, 115-155.
- Hauksson, B. (1981). Radon content of groundwater as an earthquake precursor: Evaluation of worldwide data and physical basis, *J. Geophys. Res.*, 86, B10, 9397-9410.
- Hsu, M.T. (1971). Seismicity in Taiwan and some related problems, *Bull. Intern. Inst. Seismo. Earthq. Engin.*, 8, 41-160.
- Jaume, S.C. and L.R. Sykes (1999). Evolving towards a critical point: a review of accelerating seismic moment: energy release prior to large and great earthquakes, *Pure Appl. Geophys.*, 155, 279-306.
- Kagan, Y.Y. (2002). Aftershock zone scaling, *Bull. Seism. Soc. Amer.*, 92, 2, 641-655.
- Kanamori, H. and D.L. Anderson (1975). Theoretical basis of some empirical relations in seismology, *Bull. Seism. Soc. Amer.*, 65, 1073-1095

- Kanamori, H. and T.H. Heaton (2000). Microscopic and macroscopic physics of earthquakes, in J.B. Rundle, D.L. Turcotte and W. Klein (Editors), *Geocomplexity and Physics of Earthquakes*, Am. Geophys. Monog., 120, 147-163.
- King, C.Y. (1986). Gas geochemistry applied to earthquake prediction: An overview, *J. Geophys. Res.*, 91, 12269-12281.
- King, C.Y., W. Zhang and Z. Zhang (2006). Earthquake-induced groundwater and gas changes, *Pure Appl. Geophys.*, 163, 633-645, doi:10.1007/s00024-006-0049-7.
- Knopoff, L. (1958). Energy release in earthquakes, *Geophys. J. Int.*, 1, 44-52.
- Knopoff, L. (1996). Earthquake prediction: The scientific challenge, *Proc. Nat. Acad. Sci., USA*, 93, 3719-3720.
- Konstantinos, K.I., G.A. Papadopoulos, A. Fokaefs and K. Orphanogiannaki (2005). Empirical relationships between aftershock area dimensions and magnitude for earthquakes in the Mediterranean Sea region, *Tectonophys.*, 403, 95-115.
- Kuo, T., K. Fan, H. Kuochen and W. Chen (2006a). A mechanism for anomalous decline in radon precursory to an earthquake, *Ground Water*, 44, 642-647. doi:10.1111/j.1745-6584.2006.00219.x.
- Kuo, T., C. Lin, G. Chang, K. Fan, W. Cheng and C. Lewis (2010). Estimation of aseismic crustal strain using radon precursors of the 2003 *M*_{6.8}, 2006 *M*_{6.1}, and 2008 *M*_{5.0} earthquakes in eastern Taiwan, *Natural Hazards*, 53, 219-228.
- Kuo, T., H. Kuochen, C. Ho and W. Chen (2017). A stress condition in aquifer rock for detecting anomalous radon decline precursory to an earthquake, *Pure Appl. Geophys.*, 174, 1291-1301.
- Kuo, T., W. Chen and C. Ho (2018). Anomalous decrease in groundwater radon before 2016 *M*_w6.4 Meinong earthquake and its application in Taiwan, *Appl. Radiat. Isot.*, 136, 68-72.
- Kuo, T., W. Chen, C. Lewis, C. Ho and H. Kuochen (2019). In-situ radon volatilization in an undrained fractured aquifer, *Proceed. the 44th Workshop on Geothermal Reservoir Engineering*, Stanford Univ., Calif., USA, 11-13.
- Kuo, T., W. Chen, C. Ho, H. Kuochen and C. Chiang (2020). Precursory behavior of groundwater radon in Southeastern Taiwan: Effect of tectonic setting in the subduction zone, *Pure Appl. Geophys.*, 177, 2877-2887. <https://doi.org/10.1007/s00024-019-02389-9>.
- Kuo, T., K. Fan, H. Kuochen, Y. Han, H. Chu and Y. Lee (2006b). Anomalous decrease in groundwater radon before the Taiwan *M*_{6.8} Chengkung earthquake. *J. Environ. Radio.*, 88, 101-106. <https://doi.org/10.1016/j.jenvrad.2006.01.005>.
- Liu, K.K., Y.B. Tsai, Y.H. Yeh, T.F. Yui and T.L. Teng (1984). Variations of radon content in ground waters and possible correlation with seismic activities in northern Taiwan, *Pure Appl. Geophys.*, 122, 231-244.
- Main, I.G. and P.G. Meredith (1989). Classification of earthquake precursors from a fracture mechanics model, *Tectonophys.*, 167, 273-283.
- Meng, F., L.N.Y. Wong and H. Zhou (2019). Power law relations in earthquakes from microscopic to macroscopic scales, *Sci. Rept.*, 9, 10705. <https://doi.org/10.1038/s41598-019-46864-8>.
- Minnehan, C. (2015). Newly discovered properties of elusive gamma ray flashes, *Eos, Am. Geophys. Union*, 96, doi:10.1029/2015EO032431.
- Nur, A. (1972). Dilatancy, pore fluids, and premonitory variations of *t_s/t_p* travel times, *Bull. Seism. Soc. Am.*, 62, 1217-1222.
- Omori, F. (1894). Investigation of aftershocks, *Rept. Earthquake Inv. Comm.*, 2, 103-139.
- Papazachos, C.B. and B.C. Papazachos (2001). Precursory accelerating Benioff in the Aegean area, *Ann. di Geofisica*, 44, 461-474.
- Papazachos, C.B., G.F. Karakaisis, A.S. Savvaidis and B.C. Papazachos (2002). Accelerating seismic crustal deformation in the southern Aegean area, *Bul. Seism. Soc. Am.*, 92, 570-580.
- Paudel, S.R., S.P. Banjara, A. Wagle and F.T. Freund (2018). Earthquake chemical precursors in groundwater: a review, *J. Seismol.*, 22, 1293-1314. <https://doi.org/10.1007/s10950-018-9739-8>.
- Press, F. (1967). Dimensions of the source region for small shallow earthquakes, *Proceedings of the VESIAC Conference on Shallow Source Mechanisms*, Rept. 7885-1-X, Inst. Sci. and Tech., Univ. Michigan, Ann Arbor, Michigan, USA, 155-163.
- Press, W.H., B.P. Flannery, A.A. Teukolsky and W.T. Vetterling (1986). *Numerical Recipes*, Cambridge Univ. Press Cambridge.
- Purcaru, G. and H. Berckhemer (1978). A magnitude scale for very large earthquakes, *Tectonophys.*, 49, 189-198.
- Rikitake, T. (1975a). Dilatancy model and empirical formulas for an earthquake area, *Pure Appl. Geophys.*, 113, 141-147.

- Rikitake, T. (1975b). Earthquake precursors, *Bull. Seism. Soc. Am.*, 65, 1133-1162.
- Rikitake, T. (1979). Classification of earthquake precursors, *Tectonophys.*, 54, 293-308.
- Rikitake, T. (1984). Earthquake precursors, in F.F. Evison (Editor), *Earthquake Prediction*, Terra Scientific Publishing Co., Tokyo, Unesco, Paris, 3-21.
- Rikitake, T. and Y. Yamazaki (1985). The nature of resistivity precursor, *Earthquake Pred. Res.*, 3, 559-570.
- Sarkar, I. (2010). Possible accelerated Benioff strain in the Sistan Suture Zone of eastern Iran, *Acta Geophys.*, 59, 2, 239-261. doi:10.2478/s11600-010-0051-4.
- Scholz, C.H. (1990). *The Mechanics of Earthquakes and Faulting*, Cambridge Univ. Press, Cambridge, UK, 439.
- Scholz, C.H., L.R. Sykes and Y.P. Aggarwal (1973). Earthquake prediction: A physical basis, *Science*, 181, 803-810, doi:10.1126/science.181.4102.803.
- Scordilis, E.M., C.B. Papazachos, G.F. Karakaisis and V.G. Karakostas (2004). Accelerating seismic crustal deformation before strong mainshocks in Adriatic and its importance for earthquake prediction, *J. Seismol.*, 8, 57-70.
- Segou, M. (2020). The physics of earthquake forecasting, *Seism. Res. Lett.*, 91(4), 1936-1939. doi:10.1785/0220200127.
- Shin, T.C. (1992). The calculation of local magnitude from the simulated Wood-Anderson seismograms of the short-period seismograms in the Taiwan area, *Terr. Atmos. Ocean. Sci.*, 4, 2, 155-170.
- Smith, W.D. (1981). The *b*-value as an earthquake precursor, *Nature*, 289, 136-139. doi:10.1038/289136a0.
- Smith, W.D. (1986). Evidence for precursory changes in the frequency-magnitude *b*-value, *Geophys. J. R. Astro. Soc.*, 86, 815-838.
- Tajima, F. and H. Kanamori (1985). Global survey of aftershock area expansion patterns, *Phys. Earth Planet. Inter.*, 40, 77-137.
- Teng, T.L. (1980). Some recent studies on groundwater radon content as an earthquake precursor, *J. Geophys. Res.*, 85, 3089-3099.
- Tsai, Y.B., J.Y. Liu, T.C. Shin, H.Y. Yen and C.H. Chen (2018). Multidisciplinary earthquake prediction studies in Taiwan: A review and future prospects, in D. Ouzounov, S. Pulinet, K. Hattori and P. Taylor (Editors), *Pre-Earthquake Processes: A Multidisciplinary Approach to Earthquake Prediction Studies*, Geophysical Monograph Series, 234, 41-66. <https://doi.org/10.1002/9781119156949.ch4>.
- Tsai, Y.B., T.L. Teng, Y.H. Yeh, S.B. Yu, K.K. Liu and J.H. Wang (1983). Status of earthquake prediction research in Taiwan, ROC, *Bull. Inst. Earth Sci., Acad. Sin., ROC*, 3, 1-26.
- Tsai, Y.B., J.Y. Liu, K.F. Ma, H.Y. Yen, K.S. Chen, Y.I. Chen and C.P. Lee (2004). Preliminary results of the iSTEP Program on integrated search for Taiwan earthquake precursors, *Terr. Atmos. Ocean. Sci.*, 15, 3, 345-562.
- Tsubokawa, I. (1969). On relation between duration of crustal movement and magnitude of earthquake expected. *J. Geod. Soc. Japan*, 15, 75-88. (in Japanese)
- Tsubokawa, I. (1973). On relation between duration of precursory phenomena and duration of crustal movement and magnitude before earthquake, *J. Geod. Soc. Japan*, 19, 116-119. (in Japanese)
- Tsukuda, T. (2008). Radon-gas monitoring by gamma-ray measurements on the ground for detecting crustal activity changes—Preliminary study by repeat survey method, *Bull. Earthquake Res. Inst., Tokyo Univ, Japan*, 83, 227-241.
- Utsu, T. and A. Seki (1955). A relation between the area of aftershock region and the radius of the sensibility circle, *Zisin*, 3, 44-48. (in Japanese)
- Wakita, H. (1996). Geochemical challenge to earthquake prediction, *Proc. Nat. Acad. Sci., USA*, 93, 3781-3786.
- Wakita, H., Y. Nakamura and Y. Sano (1985). Groundwater radon variations reflecting changes in regional stress fields, *Earthquake Pred. Res.*, 3, 545-557.
- Wang, J.H. and C.W. Lee (1997). Multifractal measures of time series of earthquakes, *J. Phys. Earth*, 45, 5, 331-345.
- Wang, J.H. (2004). The seismic efficiency of the 1999 Chi-Chi, Taiwan, earthquake, *Geophys. Res. Letts.*, 31, L10613. doi:10.1029/2004GL019417.
- Wang, J.H. (2009). Effect of thermal pressurization on the radiation efficiency, *Bull. Seism. Soc. Am.*, 99(4), 2293-2304.
- Wang, J.H. (2013). Memory effect in *M*₆ earthquakes of South-North Seismic Belt, Mainland China. *J. Seismol.*, 17(3), 913-924. doi:10.1007/s10950-013-9361-8.
- Wang, J.H. (2014). Memory effect in *M* ≥ 7 earthquakes of Taiwan, *J. Seismol.*, 18, 467-480. doi:10.1007/s10950-014-9420-9.
- Wang, J.H. (2016). A mechanism causing *b*-value anomalies prior to a mainshock, *Bull. Seism. Soc. Am.*, 106(1), 1663-1671, doi:10.1785/0120150335.
- Wang, J.H., K.C. Chen, P.L. Leu and C.H. Chang (2016). Precursor times of abnormal *b*-values prior to earthquakes, *J. Seismol.*, 20(3), 905-919. doi:10.1007/s10950-016-9567-7.

- Wang, J.H. (2017). Multi-stable slip in a one-degree-of-freedom spring-slider model with thermal-pressurized friction and viscosity, *Nonl. Processes Geophys.*, 24, 467-480. doi.org/10.5194/npg-24-467-2017.
- Wang, J.H. (2018). A review on scaling of earthquake faults, *Terr. Atmos. Ocean. Sci.*, 29, 6, 589-610.
- Wang, J.H. (2021a) A review on precursors of the 1999 M_w 7.6 Chi-Chi, Taiwan, earthquake, *Terr. Atmos. Ocean. Sci.*, 32(3), 275-304. doi:10.3319/TAO.2021.03.24.01.
- Wang, J.H. (2021b). A compilation of precursor times of earthquakes in Taiwan, *Terr. Atmos. Ocean. Sci.*, 32(4), 411-441. doi:10.3319/TAO.2021.07.12.01.
- Wang, K., Q.F. Chen, S. Sun and A. Wang (2006). Predicting the 1975 Haicheng earthquake, *Bull. Seism. Soc. Amer.*, 96, 757-795. doi:10.1785/0120050191.
- Whitcomb, J.H., J.D. Garmany and D.L. Anderson (1973). Earthquake prediction: Variation of seismic velocities before the San Fernando earthquake, *Science*, 180, 632.
- Woith, H. (2015). Radon earthquake precursor: A short review, *Eur. Phys. J., Special Topics*, 224, 611-627. doi:10.1140/epjst/e2015-02395-9.
- Wyss, M. (2001). Why is earthquake prediction research not progressing faster?, *Tectonophys.*, 338, 3/4, 217-223.
- Wyss, M. and J. Brune (1968). Seismic moment, stress and source dimensions for earthquakes in the California-Nevada region, *J. Geophys. Res.*, 73, 4681-4698.
- Yang, T.F., V. Walia, L.L. Chyi, C.C. Fu, C.H. Chen, T.K. Liu, S.R. Song, C.Y. Lee and M. Lee (2005). Variations of soil radon and thoron concentrations in a fault zone and prospective earthquakes in SW Taiwan, *Radiat. Meas.*, 40, 496-502.

CORRESPONDING AUTHOR: Jeen-Hwa WANG,

Institute of Earth Sciences, Academia Sinica, Taipei, Taiwan
and Department of Earth Sciences, National Central University, Jhongli, Taiwan
e-mail: jhwang@earth.sinica.edu.tw